

## Article

# Exploring Spontaneous Combustion Characteristics and Structural Disparities of Coal Induced by Igneous Rock Erosion

Mingqian Zhang <sup>1,2,3,\*</sup>, Zongxiang Li <sup>4,5</sup>, Zhifeng Chen <sup>1,2</sup>, Lun Gao <sup>1,2</sup>, Yun Qi <sup>6</sup> and Haifeng Hu <sup>7</sup>

<sup>1</sup> School of Safety Science and Engineering, Xinjiang Institute of Engineering, Urumqi 830023, China; czf@xjie.edu.cn (Z.C.); gl07@xjie.edu.cn (L.G.)

<sup>2</sup> Key Laboratory of Xinjiang Coal Mine Disasters Intelligent Prevention and Emergency Response, Xinjiang Institute of Engineering, Urumqi 830023, China

<sup>3</sup> Key Laboratory of Xinjiang Coal Resources Green Mining, Ministry of Education, Xinjiang Institute of Engineering, Urumqi 830023, China

<sup>4</sup> College of Safety Science & Engineering, Liaoning Technical University, Fuxin 123000, China; lizongxiang@lntu.edu.cn

<sup>5</sup> Key Laboratory of Mine Thermodynamic Disaster & Control of Ministry of Education, Liaoning Technical University, Huludao 125105, China

<sup>6</sup> College of Mechanical Engineering and Automation, Liaoning University of Technology, Jinzhou 121001, China; qiyun\_sx@sxdtdx.edu.cn

<sup>7</sup> Guoneng Shendong Coal Group Co., Ltd., Ordos 017200, China; 10015286@ceic.com

\* Correspondence: zmq@xjie.edu.cn

**Abstract:** The erosion of igneous rocks affects the structural and spontaneous combustion characteristics of coal. A series of tests were conducted, including programmed heating, thermogravimetric analysis, FT-IR spectroscopy, low-temperature nitrogen adsorption, and pressed mercury experiments on samples from primary coal and coal eroded by igneous rocks from the Tashan Mine and Xiaonan Mine within the same coal seam. Based on these experiments, we analyzed various properties of coal, such as the oxidation characteristics, spontaneous combustion limit, active functional group content, chemical structure, and pore structure, from both macroscopic and microscopic perspectives. The results indicated significant trends after the erosion of igneous rocks: (1) there were increases in the oxygen consumption rate, as well as the CO and CO<sub>2</sub> release rates; (2) the upper limit of air leakage intensity increased, the minimum thickness of floating coal decreased, and the lower limit of oxygen volume fraction decreased; (3) there was a decrease in the activation energy required for coal ignition; (4) there was a decrease in the active functional group content while improving the structural stability; and (5) there were the alterations in the pore structure of coal. These promoted the oxidation reactions between oxygen and the active groups within the coal matrix, increasing the propensity for spontaneous combustion, particularly in the igneous rocks with low oxidation activity.

**Keywords:** igneous rock erosion; coal spontaneous combustion; activation energy; pore structure; functional group



**Citation:** Zhang, M.; Li, Z.; Chen, Z.; Gao, L.; Qi, Y.; Hu, H. Exploring Spontaneous Combustion Characteristics and Structural Disparities of Coal Induced by Igneous Rock Erosion. *Fire* **2024**, *7*, 159. <https://doi.org/10.3390/fire7050159>

Academic Editor: Ali Cemal Benim

Received: 28 March 2024

Revised: 25 April 2024

Accepted: 28 April 2024

Published: 4 May 2024



**Copyright:** © 2024 by the authors. Licensee MDPI, Basel, Switzerland. This article is an open access article distributed under the terms and conditions of the Creative Commons Attribution (CC BY) license (<https://creativecommons.org/licenses/by/4.0/>).

## 1. Introduction

Coal remains a significant fossil fuel in the context of global energy development and utilization [1]. With increasing demand, coal mining has extended to greater depths, and the mining conditions are becoming increasingly complicated [2]. Igneous rock erosion, a common geological phenomenon, is widespread in coal-producing countries worldwide [3–7]. The erosion of igneous rocks affects the molecular structure, degree of metamorphism, pore structure, and mineral composition of coal [8–12]. The erosion of igneous rocks can lead to issues such as gas outbursts and the spontaneous combustion of coal [3,13]. Wang et al. [14] observed that the igneous rock erosion promoted the coal metamorphism, increased the coal's reflectivity, and decreased its volatile content. Yao and Liu [15] discovered that igneous rock erosion results in the formation of numerous pores during coal pyrolysis and

volatilization, thereby enhancing the coal's adsorption and desorption capacity. Additionally, Wang et al. [16], Li et al. [17], and Wu et al. [18] reported that igneous rock erosion enhanced the pore connectivity in coal, thereby elevating the risk of coal seam gas outburst disasters. Cao et al. [19] observed alterations in the geological structure of coal seams due to igneous rock erosion. Gao et al. [8] and Shi et al. [20] noted increased susceptibility to spontaneous combustion in coal samples from the Daxing mine. Although numerous studies have analyzed the impact of the changes in coal pore structure and chemical composition on gas outbursts after igneous rock erosion, there is a scarcity of systematic reports on the spontaneous combustion characteristics of coal affected by igneous rock erosion.

The widely acknowledged theory regarding spontaneous coal combustion in academia is the coal–oxygen recombination theory [21]. Ma et al. [22] assessed the severity of coal spontaneous combustion using spontaneous combustion limit parameters. Zhao et al. [23] categorized the coal combustion process into stages based on TG-DTG curves from thermogravimetric experiments and determined coal spontaneous combustion propensity based on fire temperature. Wang Jiren et al. [24] proposed a method for classifying coal spontaneous combustion tendencies using fire activation energy. Pan et al. [25] and Zhang et al. [26] utilized FTIR testing to demonstrate that higher coal metamorphic degrees correspond to lower hydroxyl group content and increased stability of aromatic hydrocarbons. Moreover, Zheng et al. [27] and Wang et al. [28] observed that the  $-CH_3$  and  $-CH_2$  groups exhibited the lowest stability and were more prone to react with  $O_2$ . Zhong et al. [29] determined through infrared diffuse reflection spectroscopy that  $-C=O-$  and  $-COOH$  groups in coal exhibited relatively high activity, while  $-C-O-$  groups remained stable. Furthermore, Li et al. [30] reported that higher rates of infrared aryl carbon, aromatic ring polycondensation, longer fat chains, and increased aromaticity correlated with higher coal grades and enhanced coal stability.

To investigate the impact of igneous rock erosion on the spontaneous combustion and structural characteristics of coal, it is essential to understand the underlying mechanisms. This study analyzed the oxidation characteristics, spontaneous combustion limits, oxidation kinetics, chemical structure, and pore characteristics of coal. The methods include temperature-programmed tests, thermogravimetric analysis, low-temperature  $N_2$  adsorption, mercury intrusion experiments, and infrared spectroscopy (FT-IR) detection, with the primary coals from the Tashan Mine and Xiaonan Mine, as well as the coal eroded by igneous rocks as the research objects. On this basis, the mechanism of mutagenicity in spontaneous coal combustion, influenced by the erosion of igneous rocks, was systematically analyzed.

## 2. Materials and Methods

### 2.1. Sample Information

The coal samples from the Tashan and Xiaonan Coal mines were selected, with original samples collected from the locations near and distant from the igneous rocks within the same coal seam. The samples from the Tashan and Xiaonan Coal mines, both in raw form and eroded by igneous rocks, were labeled as A1, A2, B1, and B2, respectively. The preparation followed the GB474-2008 standard [31], and the results of the industrial analysis are presented in Table 1.

**Table 1.** Results of industrial analysis of experimental coal samples.

Coal Sample	Proximate Analysis/%				Elemental Analysis/%					H/C
	Moisture	Ash	Volatiles	Fixed Carbon	C	H	O	N	S	
A1	5.13	11.36	33.71	49.80	79.92	5.22	13.26	1.26	0.34	0.78
A2	2.85	15.02	26.31	55.82	81.02	4.86	12.45	1.31	0.36	0.72
B1	3.55	9.47	36.48	49.50	79.85	5.36	13.49	1.01	0.29	0.81
B2	1.65	14.88	27.98	55.49	80.74	5.12	12.86	0.96	0.32	0.76

## 2.2. Analysis Methods

The impact of igneous rock erosion on the oxidation characteristics and spontaneous combustion parameters of coal was investigated using a programmed temperature detection device (Figure 1). The device consisted of a gas supply pipeline—1, a coal sample tank—2, a programmed temperature control box—3, and a gas chromatograph—4. The coal sample tank was a cylindrical steel container with dimensions of 5 cm in both inner diameter and height, containing the coal samples ranging from 0.4 to 2.4 mm in size. During the temperature program test, the coal sample tank containing the test samples was placed in a programmed temperature control box, with a temperature rise rate set at 0.5 °C/min. The gas supply pipeline provided a flow rate of 100 mL/min with an O<sub>2</sub>-N<sub>2</sub> gas mixture volume fraction of 21%. The testing temperature ranged between 30 and 180 °C. The gas composition (O<sub>2</sub>, CO, and CO<sub>2</sub>) at the exhaust end was recorded every 5 °C during heating to analyze the oxygen consumption, oxidation products, and spontaneous combustion limit parameters of the coal samples. To minimize errors, each set of experiments was conducted three times, and the average value of the three results was calculated.

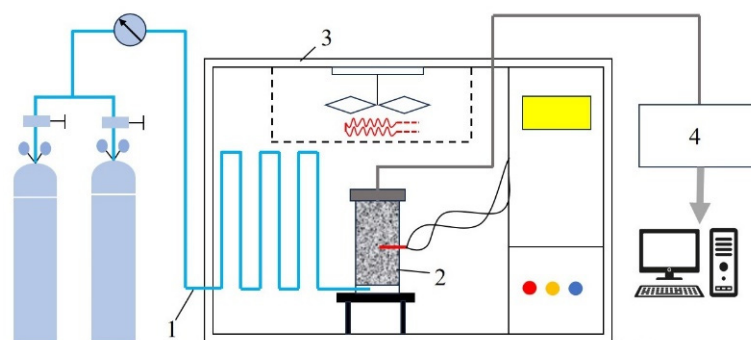


**Figure 1.** Temperature-programmed test equipment.

The thermogravimetric evaluation was conducted using an STA449C synchronous thermal analyzer (NETZSCH GMBH) manufactured by Germany NETZSCH instrument manufacturing Co., Ltd., Selbu, Germany. Each test utilized 10 mg of the coal sample with a temperature range of 30–700 °C and a heating rate of 5 °C/min. The experimental gases consisted of a mixture of N<sub>2</sub> and O<sub>2</sub>, with flow rates of 40 mL/min and 10 mL/min, respectively.

To investigate the differences of the active groups and chemical structure characteristics of coal resulting from the igneous rock erosion, the FT-IR spectrometer TENSOR27 by BRUKER in Germany was employed to analyze the coal sample at 30 °C.

The Autosorb-IQ-MP automatic specific surface area and pore size distribution analyzer from Quantachrome, Boynton Beach, FL, USA, was utilized to conduct low-temperature nitrogen adsorption experiments on coal at 77 K, and the micropores and mesoporous pores with sizes less than 50 nm were detected. The high-performance automatic mercury porosimeter (V9600, Micromeritics Corporation, Norcross, GA, USA) was applied to test the coal samples.

## 3. Results and Discussion

### 3.1. Gas Change Rate and Spontaneous Combustion Parameters

#### 3.1.1. Gas Change Rate

The calculation equation for the oxygen consumption rate is [32]

$$v_1 = \frac{Qc_0}{SL} \ln \frac{c_1}{c_2}, \quad (1)$$

where  $v_1$  is the oxygen consumption rate of the coal sample under the condition of standard oxygen molar concentration, mol/(m<sup>3</sup>·s);  $Q$  is the air flow rate in the process of programmed

temperature,  $\text{m}^3/\text{s}$ ;  $c_0$  is the volume fraction of standard  $\text{O}_2$ , 20.10%;  $c_1$  is the molar concentration of oxygen at the air inlet of the coal sample tank,  $\text{mol}/\text{m}^3$ ;  $c_2$  is the molar concentration of oxygen at the exhaust port of the coal sample tank,  $\text{mol}/\text{m}^3$ ;  $S$  is the cross-sectional area of the coal sample tank,  $\text{m}^2$ ; and  $L$  is the stacking height of the coal sample,  $\text{m}$ .

The calculation equation for the CO release rate is [33]

$$v_2 = \frac{v_1 c_3}{c_1 \left[ 1 - \exp\left(-\frac{v_1 V}{Q c_1}\right) \right]}, \tag{2}$$

where  $v_2$  represents the release rate of the coal sample under the condition that the oxygen volume fraction is  $c_1$ ,  $\text{mol}/(\text{m}^3 \cdot \text{s})$ ;  $c_3$  represents the molar concentration of CO at the exhaust port,  $\text{mol}/\text{m}^3$ ; and  $V$  denotes the volume of the experimental coal sample,  $\text{m}^3$ .

The calculation equation for the  $\text{CO}_2$  release rate is [34]

$$v_3 = \frac{v_1 c_4}{c_1 \left[ 1 - \exp\left(-\frac{v_1 V}{Q c_1}\right) \right]}, \tag{3}$$

where  $c_4$  is the molar concentration of  $\text{CO}_2$  in the exhaust port,  $\text{mol}/\text{m}^3$ .

Figure 2 illustrates the results of the temperature-programmed tests for each experimental coal sample. From Figure 2, the gas quantity fraction detected at the exhaust port of the coal sample tank exhibited an approximately exponential distribution with increasing temperature. Specifically, the oxygen quantity fraction decreased as the temperature increased, whereas the quantity fractions of CO and  $\text{CO}_2$  increased. The igneous rock erosion coal exhibited a higher consumption of oxygen volume fraction and released greater quantities of CO and  $\text{CO}_2$  volume fractions.

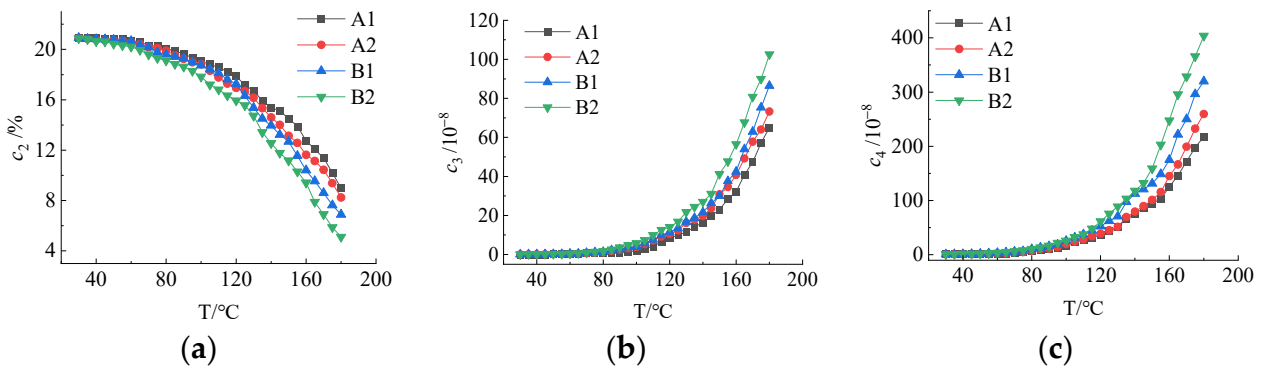


**Figure 2.** Distribution curve of the gas volume fraction: (a) oxygen volume fraction distribution curve; (b) CO volume fraction distribution curve; (c)  $\text{CO}_2$  volume fraction distribution curve.

Using Equations (1)–(3), the temperature-programmed test results of the coal samples were combined to calculate the gas change rate during coal oxidation, as shown in Figure 3. The analysis of Figure 3 revealed that the oxygen consumption, CO release, and  $\text{CO}_2$  release rates of the coal samples increased exponentially with increasing temperature. Notably, at the same temperature, the rates ( $v_1$ ,  $v_2$ , and  $v_3$ ) of igneous rock erosion of coal within the same coal seam surpassed those of primary coal.

From Figure 3a, the oxygen consumption rates of the four coal sample groups followed the sequence  $B2 > B1 > A2 > A1$  at identical temperatures. Further analyses revealed that, when influenced by igneous rock erosion within the 30–180 °C range, the  $v_1$  of sample A increased by 11.52–112.75%, and that of sample B increased by 13.70–143.74%. Figure 3b indicates that the CO release rate for sample A increased by 9.94–320.59%, and for sample B, by 1.20–50.61%. As shown in Figure 3c, the  $\text{CO}_2$  release rate for sample A increased from 1.76% to 21.82%, and for sample B, from 2.28% to 47.57%. A higher  $v_1$  corresponded

to a higher self-heating reaction rate between the coal and oxygen [35]. Additionally, the increases in the  $v_2$  and  $v_3$  characterized the enhancement of coal oxidation capacity [36]. The above test results demonstrated that igneous rock erosion can augment the oxygen consumption capacity of coal and increase the likelihood of spontaneous combustion.

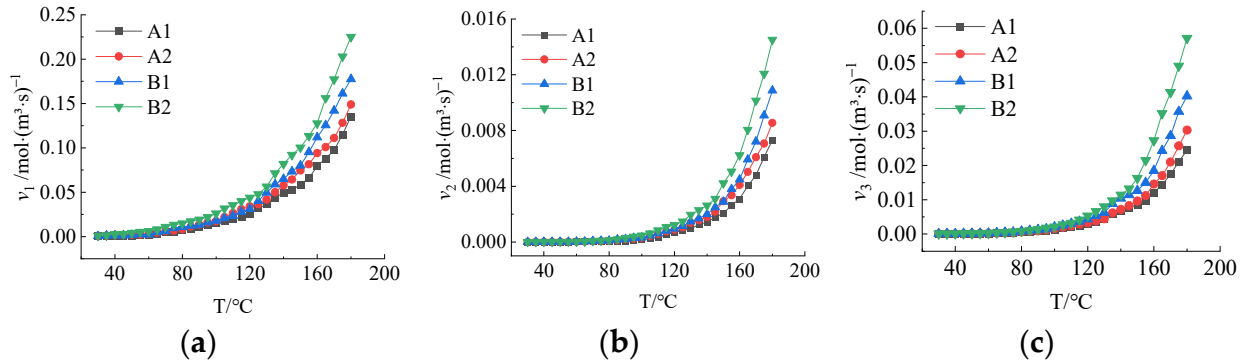


**Figure 3.** Distribution curve of the speed of gas change: (a) oxygen consumption rate fraction distribution curve; (b) CO release rate fraction distribution curve; (c) CO<sub>2</sub> release rate fraction distribution curve.

### 3.1.2. Analysis of Spontaneous Combustion Limit Parameters

The spontaneous combustion limit parameters typically encompassed the minimum floating coal thickness, lower oxygen volume fraction, and higher air leakage intensity [37,38]. When the coal thickness exceeded the minimum floating coal thickness, the quantity of oxygen available to the coal surpassed the lower limit oxygen volume fraction, and the air leakage intensity in the coal environment remained below the upper limit; heat accumulation within the coal body occurred, potentially resulting in spontaneous combustion [39–41].

The equation for calculating the minimal floating coal thickness is [42]

$$h_{\min} = \frac{\rho_g C_g Q (T - T_y) + \sqrt{(\rho_g C_g Q)^2 (T - T_y)^2 + 8 \lambda_e q (T) (T - T_y)}}{q(T)}, \quad (4)$$

where  $h_{\min}$  is the minimum thickness of the coal sample, m;  $\rho_g$  is the density of the air exposed to the coal, kg/m<sup>3</sup>;  $C_g$  is the specific heat capacity of air, J/(kg·K);  $T$  and  $T_y$  are the coal and rock temperatures, respectively, °C;  $\lambda_e$  is the thermal conductivity of coal, J/(m·s·°C); and  $q(T)$  is the exothermic intensity of oxidation when the coal temperature is  $T$ , KJ/(m<sup>3</sup>·s).

The lower oxygen volume fraction is calculated as [33]

$$c_{\min} = \frac{c_1}{q(T)} \left[ \frac{8 \lambda_e (T - T_y)}{h^2} + \rho_g C_g Q \frac{2 \times (T - T_y)}{h} \right], \quad (5)$$

where  $c_{\min}$  is the lower oxygen volume fraction, %;  $h$  is the thickness of coal, m.

The equation for calculating the upper limit of air leakage strength is [35]

$$Q_{\max} = \frac{h q(T)}{2 \rho_g C_g (T - T_y)} - \frac{4 \lambda_c}{h \rho_g C_g}, \quad (6)$$

where  $Q_{\max}$  is the upper limit of the air leakage intensity, m/s.

The exothermic intensity of the coal oxidation is calculated using Equation (7) [43].

$$q = q_a (v_1 - v_2 - v_3) + v_2 \Delta h_1 + v_3 \Delta h_2, \quad (7)$$

where  $q_a$  is the chemisorption heat of oxygen on coal, KJ/mol;  $\Delta h_1$  is the enthalpy of CO formation, kJ/mol; and  $\Delta h_2$  is the enthalpy of CO<sub>2</sub> formation, kJ/mol.

By combining the  $v_1$ ,  $v_2$ , and  $v_3$  with Equations (4)–(7), the spontaneous combustion limit parameters during the spontaneous coal combustion process were derived, with the results illustrated in Figure 4. As shown in Figure 4, as the temperature increased, the distribution trends of the  $h_{\min}$ ,  $c_{\min}$ , and  $Q_{\max}$  curves for all the tested coal samples were similar. Under identical temperature conditions, the igneous rock-eroded coal within the same coal seam exhibited lower  $h_{\min}$  and  $c_{\min}$  values and a higher  $Q_{\max}$  value than primary coal. As shown in Figure 4a, during the initial stage (<60 °C), the  $h_{\min}$  value of the test sample increased with increasing temperature, decreased rapidly within the 60–130 °C range, and then declined gradually within the 130–180 °C range. At low temperatures,  $q$  was minimally influenced by the temperature, requiring more coal oxidation and heat release to increase the temperature. Conversely, at high temperatures, the coal oxidation and heat release were significantly enhanced. At this stage, even thin coal can supply sufficient heat for coal body heating, further reducing the  $h_{\min}$  value [44]. From Figure 4b, the  $c_{\min}$  presented a trend of initially increasing and then decreasing with increasing temperature  $T$ , peaking at approximately 60 °C. This was because, during the low-temperature stage, the temperature minimally affected the coal oxidation heat production capacity, whereas it facilitated heat exchange between coal and the surrounding medium, requiring increased oxygen consumption to elevate the body temperature of the coal. Conversely, during the high-temperature stage, the temperature significantly influenced the oxidation heat production capacity of coal, allowing even a low oxygen volume fraction to satisfy the thermal balance between coal and the external environment [20]. Figure 4c illustrates that  $Q_{\max}$  initially decreased and then increased with the temperature. This contrary trend to that of  $h_{\min}$  and  $c_{\min}$  resulted from increased  $Q$ , which did not favor coal thermal storage. Therefore, to maintain the thermal balance between coal and its surroundings, the  $Q_{\max}$  initially decreased with the increasing temperature. In the high-temperature stage, the coal oxidation heat production increased significantly, necessitating a higher  $Q_{\max}$  value for thermal balance [22].

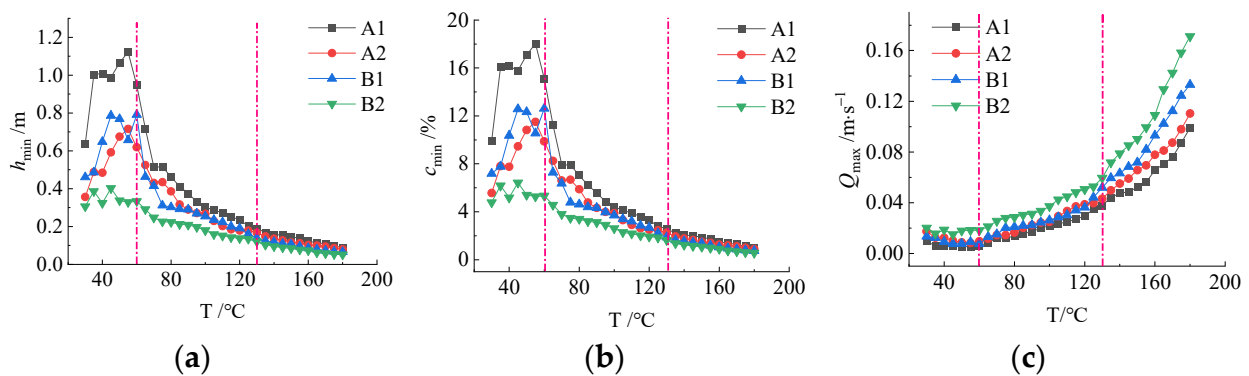


**Figure 4.** Distribution curve of spontaneous combustion limit parameters: (a)  $h_{\min}$  distribution curve; (b)  $c_{\min}$  distribution curve; (c)  $Q_{\max}$  distribution curve.

Figure 4a revealed that the coal samples eroded by the igneous rocks within the same coal seam exhibited lower  $h_{\min}$  values than the primary coal, and this difference decreased with increasing temperature. The analysis further indicated that, when influenced by the igneous rock erosion, the percentage decrease in  $h_{\min}$  in coal sample A ranged from 11.30% to 108.10%, and in coal sample B from 14.72% to 136.83% within the 30–180 °C range. This suggested that the coal eroded by igneous rocks presented better heat storage capacity than the primary coal at equivalent temperatures. As observed in Figure 4b, the percentage decrease in the  $c_{\min}$  values for coal sample A ranged from 11.32% to 110.97% and for coal sample B, from 14.77% to 139.65%. This indicated that the coal eroded by igneous rocks exhibited a higher heat production capacity than primary coal at equivalent

temperatures. Similarly, Figure 4c indicates that the increase in  $Q_{\max}$  values for coal sample A ranged from 11.30% to 108.10% and for coal sample B, from 14.72% to 136.83%. This further demonstrated the superior heat generation and storage capacity of coal eroded by the igneous rocks compared with the primary coal at the same temperature. The igneous rock erosion reduced the  $h_{\min}$  and  $c_{\min}$  that contributed to spontaneous coal combustion while enhancing the  $Q_{\max}$  capacity of floating coal. This enhancement promoted greater heat generation and accumulation within the coal body, thereby increasing the risk of spontaneous combustion.

### 3.2. Kinetic Parameters of Coal Oxidation

#### 3.2.1. Characteristic Temperature Analysis

Figure 5 illustrates the TG-DTG curves of the coal samples. At a specific temperature, certain groups within the molecular structure of coal participate in oxidation reactions [45,46]. This temperature, termed the characteristic temperature, is characterized by a noticeable change in the weight loss rate of the sample. Figure 5 illustrates five stages delineated by quality variations in the spontaneous combustion process [47], where  $S_1$  represents the evaporative desorption stage ( $T_0 - T_a$ ),  $S_2$  represents the oxygen absorption and weight gain stage ( $T_a - T_b$ ),  $S_3$  represents the thermal decomposition and weight loss stage ( $T_b - T_{ig}$ ),  $S_4$  denotes the combustion stage ( $T_{ig} - T_c$ ), and  $S_5$  denotes the burnout stage ( $>T_c$ ).

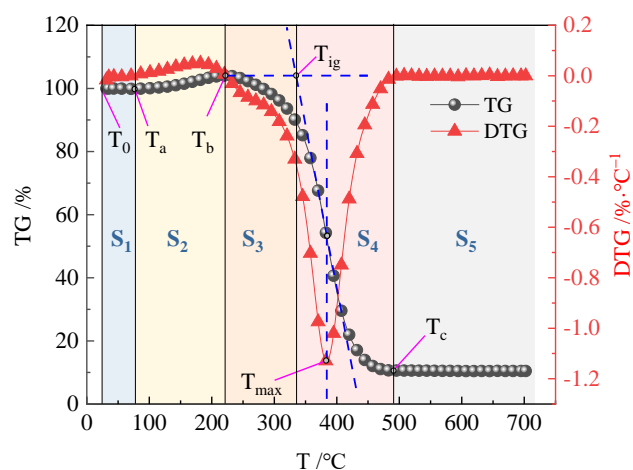


**Figure 5.** Distribution curve of spontaneous combustion parameters.

Figure 6 demonstrates the TG-DTG curves of the four test coal samples, and the characteristic temperature results are recorded in Table 2. Table 2 illustrates a 39.84% decrease in the activation temperature ( $T_a$ ) for coal A and a 14.67% decrease for coal B owing to igneous rock erosion. This was attributed to the acceleration of structural side-chain fractures and coal pyrolysis resulting from igneous rock erosion [47]. Furthermore, the percentage decreases in the ignition temperature ( $T_{ig}$ ) were 1.89% and 2.10%, respectively, indicating that the igneous rock erosion enhanced the spontaneous combustion tendency of coal. Similarly, the percentage decreases in the rate of maximum weight loss temperature ( $T_{max}$ ) were 2.30% and 1.189%, respectively, suggesting that the igneous rock erosion promoted the formation of active groups in coal, accelerating the oxidation reaction rate and exothermic rate [47]. Additionally, the percentage decreases in burnout temperature ( $T_c$ ) were 0.88% and 2.31%, respectively. Compared to the primary coal, the coal samples eroded by the igneous rocks exhibited varying degrees of decrease in characteristic temperature. This erosion enhanced the oxidation reaction and gas diffusion ability of the coal.

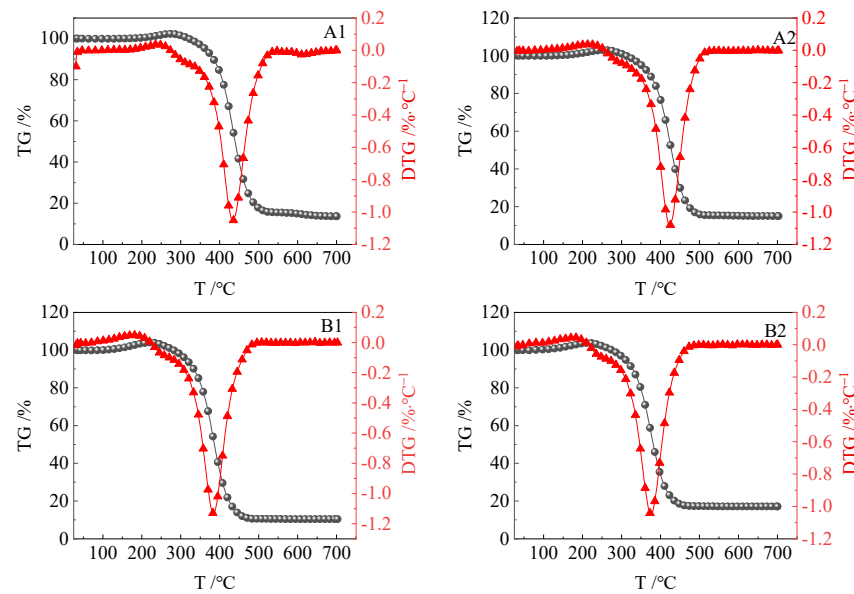


Figure 6. Distribution curve of TG-DTG.

Table 2. Characteristic temperatures of combustion of coal samples.

Coal Sample	T <sub>0</sub> /°C	T <sub>a</sub> /°C	T <sub>b</sub> /°C	T <sub>ig</sub> /°C	T <sub>max</sub> /°C	T <sub>c</sub> /°C
A1	31.19	113.09	273.23	387.96	432.86	549.45
A2	31.59	68.04	260.96	380.63	422.92	544.63
B1	31.44	74.02	222.63	335.41	380.07	514.97
B2	31.27	63.16	212.23	328.36	375.55	503.06

### 3.2.2. Activation Energy Analysis

The most commonly used kinetic equation to describe non-isothermal and non-homogeneous reactions is [48]

$$\frac{d\alpha}{dT} = \left(\frac{1}{\beta}\right) \cdot k(T) \cdot f(\alpha), \tag{8}$$

where  $\alpha$  represents the conversion rate, %;  $T$  represents the thermodynamic temperature, K;  $\beta$  denotes the heating rate, K/min;  $k(T)$  denotes the reaction rate constant; and  $f(\alpha)$  denotes a function of the reaction mechanism.

The empirical equation proposed by Arrhenius for the variation in the reaction rate constant with temperature is commonly utilized to express the reaction rate constant  $k$ .

$$k = A \exp\left(-\frac{E}{RT}\right), \tag{9}$$

where  $E$  is the reaction activation energy, kJ/mol.

By combining Equations (8) and (9), we derived the kinetic equations of heterogeneous systems under isothermal and non-isothermal conditions, respectively.

$$\frac{d\alpha}{dT} = A \exp\left(-\frac{E}{RT}\right) \cdot f(\alpha), \tag{10}$$

$$\frac{d\alpha}{dT} = \left(\frac{A}{\beta}\right) \exp\left(-\frac{E}{RT}\right) \cdot f(\alpha), \tag{11}$$

Equation (11) can be shifted, integrated, and applied to calculate the conversion rate from  $\alpha_0$  to  $\alpha_n$ , with the temperature ranging from  $T_0$  to  $T_n$  as follows:

$$\int_{\alpha_0}^{\alpha_n} \frac{d(\alpha)}{f(\alpha)} = \frac{A}{\beta} \int_{T_0}^{T_n} \exp\left(-\frac{E}{RT}\right) dT, \tag{12}$$

The left integral form of the definition Equation (12) is

$$G(\alpha) = \int_{\alpha_0}^{\alpha_n} \frac{d(\alpha)}{f(\alpha)}, \tag{13}$$

Equation (12) can be treated using the Coats–Redfern method, and the approximate integral expression of the coal oxidation kinetic equation is obtained:

$$\ln\left[\frac{G(\alpha)}{T^2}\right] = \ln\left(\frac{A \cdot R}{\beta \cdot E}\right) - \frac{E}{R \cdot T}, \tag{14}$$

Utilizing the Arrhenius formula and Equation (14), the experimental coal samples were plotted on a coordinate axis, with  $1/T$  as the abscissa and  $\ln[G(\alpha)/T^2]$  as the ordinate. The linear segments were then fitted to the plotted points, allowing the determination of the reaction activation energy  $E$ . The reaction mechanism function,  $G(\alpha)$ , is defined as  $G(\alpha) = -\ln(1 - \alpha)$ . Figure 7 and Table 3 present the fitted line segment results and the corresponding activation energy calculations, respectively.

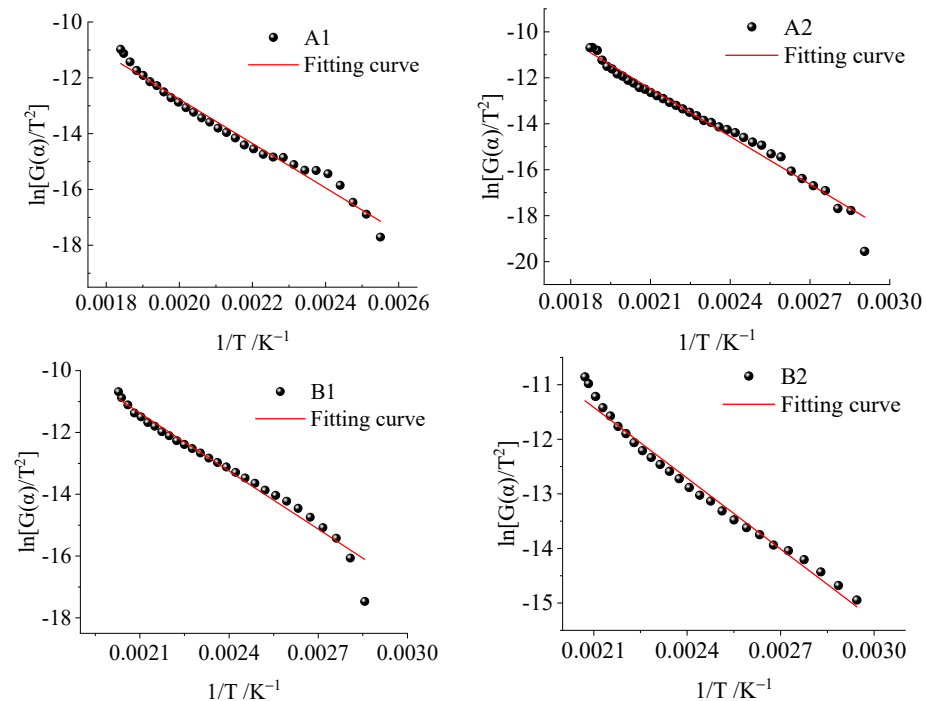


Figure 7. Fitting curve of activation energy of coal samples.

Table 3. Calculation results of ignition activation energy of coal samples.

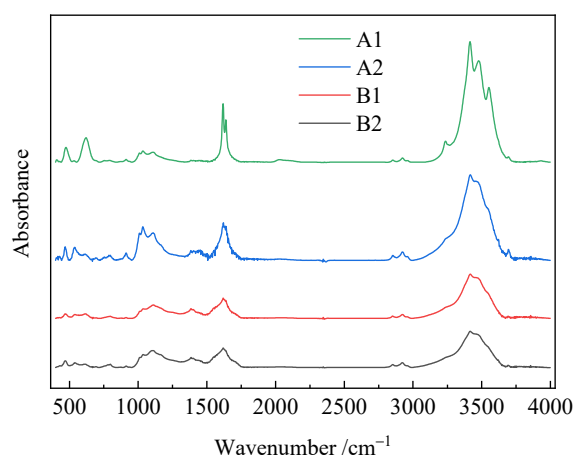
Coal Sample	E/KJ.mol <sup>-1</sup>	R <sup>2</sup>	Coal Sample	E/KJ.mol <sup>-1</sup>	R <sup>2</sup>
A1	66.1213	0.9767	A2	57.6178	0.9790
B1	52.0858	0.9740	B2	35.9615	0.9831

Figure 7 and Table 3 depict the linear relationships of each experimental coal sample, using  $G(\alpha) = -\ln(1 - \alpha)$  as the reaction mechanism function, revealing correlation coefficients ( $R^2$ ) exceeding 0.97. The ignition activation energy for sample A1 was  $66.1213 \text{ kJ mol}^{-1}$ , while for the A2, it was  $57.6178 \text{ kJ mol}^{-1}$ , representing a 12.86% decrease. Sample B1 exhibited an activation energy of  $52.0858 \text{ kJ mol}^{-1}$ , while for B2, it was  $35.9615 \text{ kJ mol}^{-1}$ , reflecting a 30.96% decrease. Compared with primary coal, the coal eroded by the igneous rocks presented a heightened propensity for exothermic oxidation reactions.

### 3.3. FT-IR Analysis of Coal Samples

#### 3.3.1. Functional Group Content Analysis

The infrared spectrum curves of the four groups of experimental coal samples are shown in Figure 8.



**Figure 8.** FTIR spectral of coal samples.

To examine the influence of igneous rock erosion on the surface functional group content of coal, the infrared spectral curves of the four coal sample groups (Figure 8) were analyzed using peak fitting software. The peak areas corresponding to the main functional groups of each coal sample were calculated, and the resulting peak-fitting curves are shown in Figure 9. The detailed fitting results are listed in Table 4.

Table 4 revealed notable changes in the functional group contents of coal samples A and B affected by igneous rock erosion. The aromatic hydrocarbon content increased by 54.72% and 471.65% in the coals A and B, respectively. The oxygen-containing functional group content increased by 50.15% and 16.83%, and the aliphatic hydrocarbon content increased by 54.22% and 30.01%, respectively. Conversely, the hydroxyl content decreased by 19.41% and 15.29%, respectively. The infrared spectral analysis suggested that the thermal erosion from the igneous rocks decomposed organic matter and released volatile compounds, resulting in changes in the composition of the active functional groups of coal [8,49]. Specifically, the aromatic hydrocarbons, oxygen-containing functional groups, and aliphatic hydrocarbon contents increased while the hydroxyl group content decreased. However, the extremely low  $-\text{COOH}$  content detected was not evident in the infrared spectrum and was therefore not analyzed. A comparison of the relative content of  $-\text{C}=\text{O}$  within the oxygen-containing functional groups across different coal samples revealed significant changes. In coal A, the relative content of  $\text{C}=\text{O}$  decreased from 16.20% to 5.82%, indicating a substantial decrease of 64.07%. Similarly, in the coal B, it decreased from 5.41% to 5.23%, representing a decrease of 3.33%. This reduction weakened the oxidizing activity of coal owing to the igneous rock erosion. The aliphatic hydrocarbons in coal, primarily comprising  $-\text{CH}_3$  and  $-\text{CH}_2$ , reacted with oxygen during coal oxidation, producing highly active  $-\text{OH}$  groups that were easily oxidized [50]. Table 4 demonstrated that the coal eroded by the igneous rocks within the same seam exhibited a higher aliphatic hydrocarbon

content and lower hydroxyl content than primary coal. This phenomenon may result from thermal metamorphism induced by igneous intrusions, which reduced the ability of aliphatic hydrocarbons to generate -OH groups [49,51]. Consequently, the reduced -OH content in coal weakened its oxidation activity.

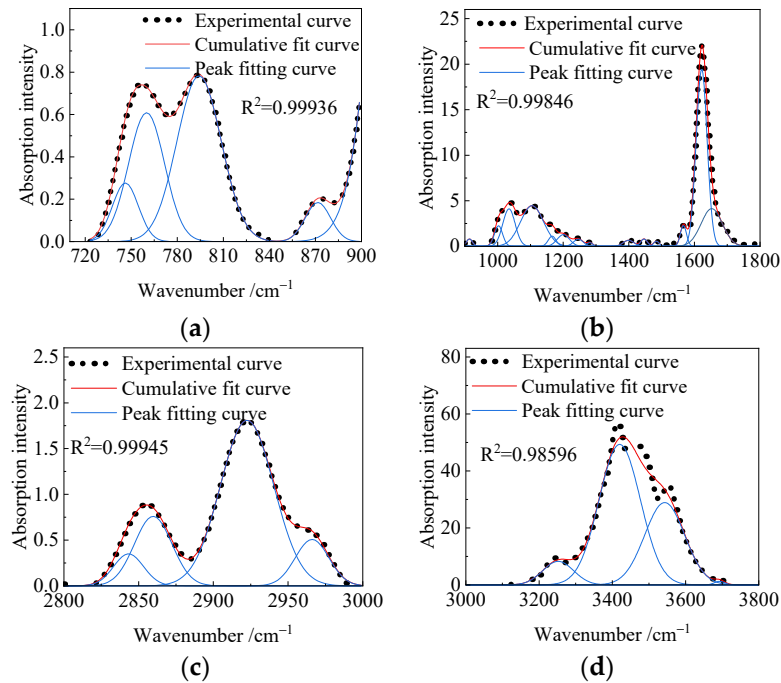


**Figure 9.** Peak fitting diagram of infrared spectra of coal samples: (a) aromatic hydrocarbon; (b) oxygen-containing functional group; (c) aliphatic hydrocarbon; (d) hydroxyl.

**Table 4.** Infrared absorption peak area proportions of main functional groups in coal samples.

Coal Sample	Aromatic Hydrocarbon/%	Oxygen-Containing Functional Group/%	Aliphatic Hydrocarbon/%	Hydroxyl/%
A1	0.44	14.62	0.91	84.04
A2	0.97	29.33	1.98	67.73
B1	0.71	34.97	1.56	62.77
B2	0.97	42.39	2.05	54.60

### 3.3.2. Chemical Structure Analysis of Coal

The infrared aromatic carbon rate ( $f_a$ ), condensation degree (DOC) of the aromatic ring, aromatic chain length ( $\text{CH}_2/\text{CH}_3$ ), and aromaticity (I) of coal can be calculated by integrating the peak fitting results using the following equations [30].

The infrared aromatic carbon content of the coal samples was calculated using the following equation:

$$f_a = 1 - \frac{C_{al}}{C}, \quad (15)$$

$$\frac{C_{al}}{C} = \left( \frac{H_{al}}{H} \times \frac{H}{C} \right) / \frac{H_{al}}{C_{al}}, \quad (16)$$

$$\frac{H_{al}}{H} = \frac{H_{al}}{H_{al} + H_{ar}} = \frac{A_{3000-2800}}{A_{3000-2800} + A_{900-700}}, \quad (17)$$

where  $C_{al}$  is the fatty carbon content in coal, %;  $C$  is the total carbon content in coal, %;  $H_{al}$  is the fatty hydrogen content in coal, and  $H$  is the total hydrogen content in coal, %;  $H_{al}$  is the hydrogen atom content in aliphatic hydrocarbons in coal, %;  $C_{al}$  is the carbonogen content in aliphatic hydrocarbon in coal, %;  $H_{al}/C_{al}$  usually takes the empirical value of

1.8;  $H_{al}$  is the relative content of aliphatic hydrogen substances in coal samples;  $H_{ar}$  is the relative content of aromatic hydrogen substances in coal samples; and  $A_{3000-2800}$  and  $A_{900-700}$  are the peak areas of the aliphatic and aromatic ring substitution zones in the fitting results, respectively.

The degree of aromatic ring condensation in coal samples can be quantified by the ratio of the vibration intensity of the aromatic ring substitution zone to the aromatic hydrocarbon C=C near  $1600\text{ cm}^{-1}$ , as computed using the formula [52]:

$$\text{DOC} = \frac{A_{900-700}}{A_{1600}}, \quad (18)$$

The value of  $\text{CH}_2/\text{CH}_3$  serves as an indicator of the aromatic chain length in coal samples, with a higher value indicating a longer fatty chain. This calculation was performed using the following equation [53].

$$\frac{\text{CH}_2}{\text{CH}_3} = \frac{A(\text{CH}_2)}{A(\text{CH}_3)} = \frac{A_{2850-2835}}{A_{2876-2858}}, \quad (19)$$

The aromaticity ( $I$ ) reflects the abundance of aromatic compounds relative to aliphatic compounds in coal. This calculation was performed using the following equation [54]:

$$I = \frac{A_{900-700}}{A_{3000-2800}} \quad (20)$$

The peak areas of the main functional groups in the experimental coal samples were determined based on the peak fitting results (Table 5). The structural parameters of the FTIR spectra for the coal samples were derived by combining the data from Table 5 with Equations (15)–(20), with the corresponding calculations provided in Table 6.

**Table 5.** Peak area distribution of main functional groups in coal.

Coal Sample	$A_{900-700}$	$A(\text{C}=\text{C})$	$A(\text{C}=\text{O})$	$A(\text{CH}_2)$	$A(\text{CH}_3)$	$A_{3000-2800}$
A1	61.5798	822.7195	333.6664	80.9893	14.2851	127.8715
A2	145.94258	1167.4645	258.1762	182.4507	31.0385	299.6164
B1	58.1469	470.3174	155.2843	77.6118	13.8259	128.1153
B2	77.0079	574.4442	177.0478	96.6709	17.1441	163.3034

**Table 6.** Structural parameters from FTIR calculation.

Coal Sample	$f_a$	DOC	$\text{CH}_2/\text{CH}_3$	$I$
A1	0.7061	0.0748	5.6695	0.4816
a2	0.7311	0.1250	5.8782	0.48714
B1	0.6922	0.1236	5.6135	0.45390
B2	0.7127	0.1341	5.6387	0.47156

Owing to igneous rock erosion, the  $f_a$  values of samples A and B increased by 3.54% and 2.96%, respectively, indicating an increase in the aromatic carbon content and enhancement of coal aromaticity. Moreover, the DOC values increased by 67.11% and 8.50%, respectively, and the degree of aromatic ring polycondensation increased [55]. Additionally, the increase in  $\text{CH}_2/\text{CH}_3$  values by 3.68% and 0.45%, respectively, suggested a higher degree of coal branching, with unstable components transforming into stable components [56]. Furthermore, the increase in aromaticity ( $I$ ) by 1.15% and 3.89%, respectively, due to igneous rock erosion, implies an elevation in the rank of coal [30].

The results of the infrared spectrum test revealed that the thermal metamorphism induced by the igneous intrusions led to several notable changes in the coal composition. These included an increase in the contents of aromatic hydrocarbons, oxygen-containing

functional groups, and aliphatic hydrocarbons, along with a decrease in the hydroxyl group content and the relative content of active groups such as  $-C=O-$ . These alterations resulted in reduced coal oxidation activity. Additionally, an enhancement was observed in the coal aromaticity, degree of condensation, and degree of branched-chaining, contributing to an increased content of the aromatic structure within the coal and an enhancement of its structural stability.

### 3.4. Specific Surface Area and Pore Distribution of Coal

The microporous and mesoporous pore size distributions of the coal samples are shown in Figure 10. From Figure 10, both igneous eroded coal and primary coal exhibited similar distribution trends in micropores and mesopores. Specifically, in Figure 10a,b, the distribution curves of micropores and mesopores for both types of coal within the same seam presented a multi-peak distribution, with the primary peak centered approximately 0.6 nm. Notably, the main peak in the distribution curve of the igneous eroded coal was notably lower than that of the primary coal. Furthermore, Figure 10c,d illustrate that the distribution curve of the mesopore diameter for both types of coal within the same seam followed a single-peak distribution pattern, with pore diameters primarily concentrated in the 2–10 nm range. However, for pore sizes larger than 19 nm, the distribution curve of the mesoporous pore size for igneous eroded coal exceeded that of primary coal. This discrepancy may stem from the thermal effects on the coal during igneous rock erosion, potentially leading to the disruption of bottleneck holes within the coal samples and resulting in a reduction in bottleneck holes [12,57].

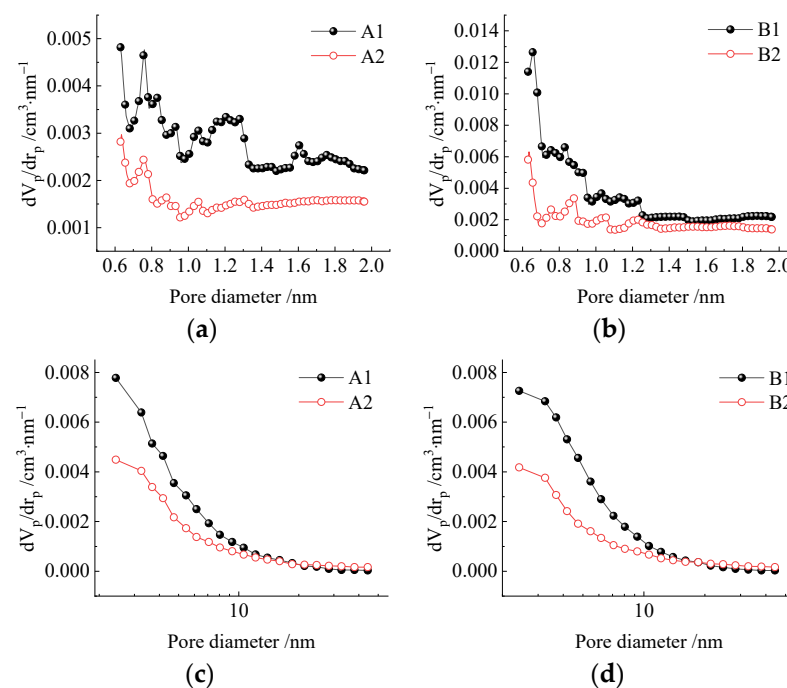


**Figure 10.** Pore size distribution characteristics of coal samples: (a) micropores in coal sample A; (b) micropores in coal sample B; (c) mesopores in coal sample A; (d) mesopores in coal sample B.

The pore structure parameters of the coal samples obtained via  $N_2$  adsorption are listed in Table 7. These parameters included the specific surface area and average pore diameter, determined using the BET calculation model; the micropore pore volume obtained via the HK calculation model; and the mesopore pore volume, calculated using the BJH model. As a consequence of the igneous rock erosion, the specific surface area ( $S_p$ ) of samples A and B decreased by 68.47% and 46.35%, respectively, while the average pore diameter increased by 30.94% and 50.51%, respectively. Moreover, the micropore pore volume ( $V_{mic}$ ) decreased by 62.06% and 54.39%, and the mesopore pore volume decreased by 26.35% and

32.11%, respectively. Previous research by Shi [21] and Jiang [58] highlighted the dominance of micropores and mesopores in determining the specific surface area of coal, and their evolution significantly influenced this parameter. Consequently, igneous rock erosion led to a reduction in the specific surface area and pore volume of micropores and mesopores in coal, accompanied by an increase in the average pore diameter, thereby altering the original pore structure characteristics of the micropores and mesopores in coal.

**Table 7.** Pore structure parameters of coal samples obtained by N<sub>2</sub> adsorption.

Coal Sample	BET		Pore Volume	
	Specific Surface Area/(m <sup>2</sup> ·g <sup>-1</sup> )	Average Pore Diameter/nm	HK Micropore Volume/×10 <sup>-3</sup> (cm <sup>3</sup> ·g <sup>-1</sup> )	BJH Mesopore Volume/×10 <sup>-3</sup> (cm <sup>3</sup> ·g <sup>-1</sup> )
A1	14.43	5.67	4.27	18.29
A2	4.55	8.21	1.62	13.47
B1	17.39	5.34	6.38	19.40
B2	9.33	10.79	2.91	13.17

To investigate the impact of igneous rock erosion on the macroscopic pore structure of coal, the coal samples were tested using a mercury intrusion meter. The relationship between the pore size distribution and mercury intake at various stages is illustrated in Figure 11. The analysis in Figure 11 revealed a decline in the mercury intake curve for both the igneous eroded coal and primary coal samples as the pore size increased. However, when the pore size exceeded 20 nm, the mercury intake curve for igneous erosion coal notably surpassed that of the primary coal, which was consistent with previous findings reported in the literature [20]. This suggested that hydrocarbon gases, such as CH<sub>4</sub>, generated through the thermal erosion of coal during igneous rock erosion, contribute to the formation of larger pores within the coal structure [51,59].

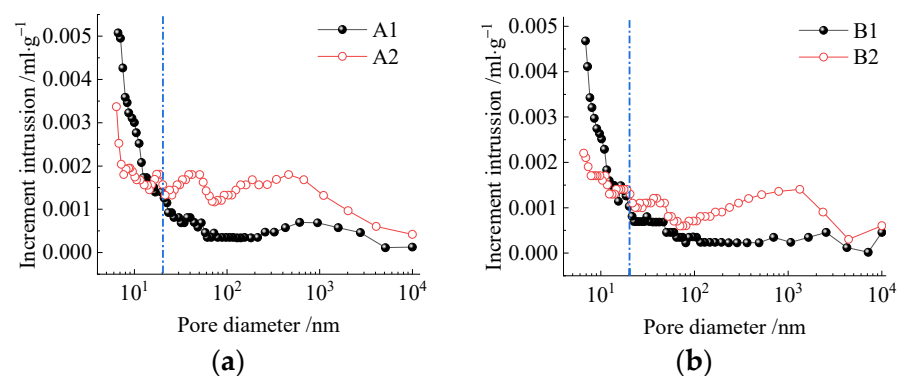


**Figure 11.** Relation curve between the pore size distribution and stage mercury intake of coal: (a) relationship between pore size distribution of coal sample A and mercury intake at different stages; (b) relationship between pore size distribution of coal sample B and mercury intake at different stages.

The specific surface area ( $S_p$ ) and pore volume distribution for mesopores and macropores in the coal samples are presented in Table 8. The analysis of the mercury injection experimental results revealed that, when influenced by the igneous rock erosion, the  $S_p$  of mesopores decreased by 21.37% for both samples A and B. Conversely, the specific surface areas of the macropores increased by 73.13% and 57.57%, respectively. Furthermore, the pore volume of the mesopores decreased by 3.96% and 7.41% for samples A and B, respectively, whereas the pore volume of the macropores increased by 66.46% and 66.04%, respectively. These findings indicated that while igneous rock erosion led to a reduction in the specific surface area and pore volume of mesopores in coal, there is a noticeable increase in pore volume, average pore size, and specific surface area for pores

with diameters > 20 nm, resulting in a significant enhancement in the average pore size, macropore volume, and macropore  $S_p$  of coal.

**Table 8.** Results of pore structure parameters of coal samples.

Coal Sample	Specific Surface Area/(m <sup>2</sup> ·g <sup>-1</sup> )		Pores Volume/(cm <sup>3</sup> ·g <sup>-1</sup> )	
	Mesoporous	Macropores	Mesoporous	Macropores
A1	22.1051	0.2780	0.0606	0.0109
A2	17.3817	1.0347	0.0582	0.0325
B1	17.9801	0.2377	0.0499	0.0072
B2	14.1379	0.5602	0.0462	0.0212

Based on the results of low-temperature nitrogen adsorption and mercury intrusion experiments, the igneous rock erosion disrupted and collapsed the original micro- and mesopores within coal, creating larger pore pathways. The thermal erosion of coal generated hydrocarbon gases that increased the proportion of pores exceeding 20 nm in diameter, augmenting the specific surface area and pore volume of macropores and facilitating gas diffusion within the pore structure [60–62]. This alteration in the pore structure due to igneous erosion promoted greater oxygen infiltration and interaction with active sites on the coal pore surfaces, thereby accelerating coal oxidation and self-heating reactions, consequently increasing the risk of coal oxidation and spontaneous combustion.

### 3.5. Difference Analysis of Spontaneous Combustion of Igneous Eroded Coal

The oxidation and spontaneous combustion of coal can be influenced by both internal and external factors. Internally, certain factors such as the coal rank, weathering, inherent moisture, sulfur content, composition, particle size, pore structure, and gas content can play crucial roles. Geological conditions, mining techniques, temperature, oxygen availability, atmospheric humidity, and ventilation management are significant external factors. In this study, four coal sample groups were prepared and tested under uniform conditions to minimize differences in particle size and external factors. Specifically, the igneous rock erosion enhanced the coal body's oxygen consumption capacity, reduced the  $h_{\min}$  and  $c_{\min}$  values, increased the  $Q_{\max}$  values, and lowered the characteristic temperature and ignition activation energy, ultimately rendering the coal more susceptible to spontaneous combustion at a macroscopic level. However, the coal samples eroded by igneous rocks exhibit a decrease in the content of highly reactive functional groups, such as -C=O- and -OH, coupled with an increase in aromatic carbon content, polycondensation, and branching, thus enhancing the structural stability of coal. At the microscopic chemical structure level, the igneous rock erosion reduced the coal oxidation activity, impeding its exothermic reaction. The macro-level findings from programmed temperature experiments and thermogravimetric analysis regarding the impact of igneous rock erosion on coal oxidation and spontaneous combustion were inconsistent with the micro-chemical structure results obtained from the FT-IR analysis. As depicted in Figure 12, the thermal metamorphism induced by igneous intrusions decomposes and transforms organic matter in coal, thereby reducing its oxidation activity. Additionally, these intrusions alter the pore structure of coal. The decomposition and collapse of the micropores and mesopores in coal, along with the creation of larger pore pathways, enhanced the surface area of coal. This facilitated the entry of oxygen into the coal mass, replacing the original gases, such as CH<sub>4</sub> adsorbed within the coal. Consequently, oxygen interacted with active coal groups, leading to combustion with reduced oxidation activity.

In actual mining operations, the coal near igneous rocks within the same seam is more prone to spontaneous combustion [20]. The igneous rock erosion not only enhances the intrinsic oxidation and heat release capabilities of coal but also correlates significantly with external factors such as geological conditions, mining techniques, and air leakage intensity. The igneous rock erosion complicates coal extraction, decelerates the working face

advancement, and prolongs coal–oxygen contact near igneous formations. The weakened integrity of the coal eroded by the igneous rocks leads to increased fragmentation during mining, resulting in more coal remnants in the goaf. These remnants act as reactants for coal oxidation and spontaneous combustion. Additionally, the hardness of igneous rocks prevents easy collapse in the goaf, reducing compaction and increasing goaf porosity. This facilitates the airflow penetration from the working face into the deeper goaf regions. Furthermore, the coal seams affected by igneous intrusion typically exhibit a higher gas content than ordinary seams [63,64]. When igneous rocks erode coal and cause fractures, the gas previously stored in the coal is displaced by oxygen, thereby facilitating coal oxidation upon contact [15]. Several strategies are commonly employed to mitigate the risk of gas-related incidents during mining in coal seams. These include drilling and pumping holes, establishing pumping roadways, and augmenting the airflow to the working face to lower gas concentrations. However, these measures inadvertently introduce significant airflow into the goaf, which can exacerbate spontaneous coal combustion [65]. Apart from the chemical composition, microcrystalline structure, and pore characteristics of coal, other factors that influence its susceptibility to spontaneous combustion include moisture levels, particle size, geological conditions, mining techniques, and ventilation strategies. Consequently, further investigations should utilize alternative methodologies to assess how these factors contribute to the risk of spontaneous coal combustion.

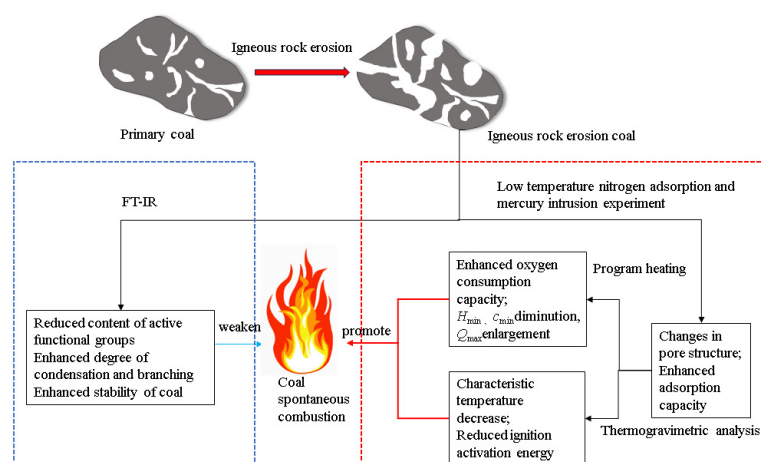


**Figure 12.** Mechanism of spontaneous combustion of coal induced by igneous rock erosion.

#### 4. Conclusions

This study examined the impact of igneous intrusions on the spontaneous combustion characteristics and structure of coal. Through temperature-programmed tests, thermogravimetric analysis experiments, FT-IR tests, low-temperature nitrogen adsorption experiments, and mercury injection experiments, the following conclusions were drawn:

(1) Igneous rock erosion heightened the oxygen consumption capacity of coal, diminished  $h_{\min}$  and  $c_{\min}$ , and amplified  $Q_{\max}$ , thereby elevating the risk of spontaneous combustion. After the igneous rock erosion, samples A and B exhibited increases in  $v_1$  by 11.52–112.75% and 13.70–143.74%, respectively, across the temperature range of 30–180 °C. Similarly,  $v_2$  increased by 9.94–320.59% and 1.20–50.61%, and  $v_3$  increased by 1.76–21.82% and 2.28–47.57%, respectively. Furthermore,  $h_{\min}$  decreased by 11.30–108.10% and 14.72–136.83%,  $c_{\min}$  decreased by 11.32–110.97% and 14.77–139.65%, and  $Q_{\max}$  increased by 11.30–108.10% and 14.72–136.83%, respectively.

(2) The igneous rock erosion lowered the characteristic temperature for spontaneous coal combustion, decreased the coal ignition activation energy, and heightened its spontaneous combustion propensity. Following the igneous rock erosion, the activation temperatures  $T_a$  of samples A and B decreased by 39.84% and 14.67%, respectively. In addition, the maximum mass temperature  $T_b$  decreased by 4.49% and 4.67%,  $T_{ig}$  decreased by 1.89%

and 2.10%, and  $T_{\max}$  decreased by 2.30% and 1.189%, respectively. Moreover, the activation energy of samples A and B decreased by 12.86% and 30.96%, respectively.

(3) The igneous thermal erosion decreased the -C=O- and -OH contents in the coals, enhancing their structural stability and reducing their oxidizing activity. Under igneous rock erosion, the relative content of -C=O- decreased by 64.07% and 3.33%, and the decreases in relative -OH content were 19.41% and 15.29%, respectively, in samples A and B, leading to weakened coal oxidizing activity. Additionally, the fa value increased by 3.54% and 2.96%, and the DOC value increased by 67.11% and 8.50% in samples A and B, respectively. The  $\text{CH}_2/\text{CH}_3$  value increased by 3.68% and 0.45%, and the I value increased by 1.15% and 3.89%, respectively, enhancing the structural stability of the coal.

(4) The igneous rock erosion altered the pore structure characteristics of coal, enhancing its exothermic oxidation reaction and exacerbating its spontaneous combustion tendency despite its low oxidation activity. As a result of the igneous rock erosion, the  $S_p$  of the mesopores decreased by 21.37% for samples A and B, respectively, while the specific surface area of macropores increased by 73.13% and 57.57%, respectively. The pore volume of the mesopores decreased by 3.96% and 7.41%, respectively, and the pore volume of the macropores increased by 66.46% and 66.04%, respectively. Furthermore, there was a notable increase in the proportion of pore structures larger than 20 nm, facilitating oxygen penetration into the coal body and enhancing the reaction with active groups, thereby amplifying the spontaneous combustion tendency of low-oxidation igneous rocks.

**Author Contributions:** Conceptualization, Z.L. and M.Z.; methodology, Z.L.; validation, M.Z. and Z.C.; formal analysis, H.H.; investigation, L.G.; resources, H.H. and Y.Q.; data curation, M.Z.; writing—original draft preparation, M.Z.; writing—review and editing, L.G.; funding acquisition, Z.L. and M.Z. All authors have read and agreed to the published version of the manuscript.

**Funding:** This research was supported by the Key Laboratory of Xinjiang Coal Resources Green Mining, Ministry of Education (KLXGY-Z2405), and the National Natural Science Foundation of China (Grant No. 51774170).

**Data Availability Statement:** The data required for this study are contained in the manuscript and are always available without limitation.

**Acknowledgments:** Thanks to the staff of Xiaonan Coal Mine and Tashan Coal Mine for collecting and testing coal samples for this study.

**Conflicts of Interest:** Author Haifeng Hu was employed by the Guoneng Shendong Coal Group Co., Ltd. The remaining authors declare that the research was conducted in the absence of any commercial or financial relationships that could be construed as a potential conflict of interest.

## References

1. Wang, C.; Wu, S.; Lv, Q.; Liu, X.; Chen, W.; Che, D. Study on correlations of coal chemical properties based on database of real-time data. *Appl. Energy* **2017**, *204*, 1115–1123. [[CrossRef](#)]
2. Liu, L.; Zhou, F.-B. A comprehensive hazard evaluation system for spontaneous combustion of coal in underground mining. *Int. J. Coal Geol.* **2010**, *82*, 27–36. [[CrossRef](#)]
3. Jiang, J.; Zhao, K.; Cheng, Y.; Zheng, S.; Zhang, S.; Wang, R. Numerical simulation of magma intrusion on the thermal evolution of low-rank coal. *Environ. Earth Sci.* **2021**, *80*, 562. [[CrossRef](#)]
4. Dutcher, R.R.; Campbell, D.-L.; Thornton, C.P. Coal metamorphism and igneous intrusions in Colorado. *Adv. Chem.* **1966**, *55*, 708–723. [[CrossRef](#)]
5. Finkelman, R.-B.; Bostick, N.-H.; Dulong, F.-T.; Senftle, F.E.; Thorpe, A.N. Influence of an igneous intrusion on the inorganic geochemistry of a bituminous coal from Pitkin County, Colorado. *Int. J. Coal Geol.* **1998**, *36*, 223–241. [[CrossRef](#)]
6. Wang, L.; Cheng, L.-B.; Cheng, Y.-P.; Yin, G.-Z.; Cai, C.-C.; Xu, C.; Jin, K. Thermal effects of magmatic sills on coal seam metamorphism and gas occurrence. *Bull. Volcanol.* **2014**, *76*, 1411–1422. [[CrossRef](#)]
7. Aarnes, I.; Svensen, H.; Polteau, S.; Planke, S. Contact metamorphic devolatilization of shales in the Karoo Basin, South Africa, and the effects of multiple sill intrusions. *Chem. Geol.* **2011**, *281*, 181–194.
8. Gao, Y.; Qin, B.; Shi, Q.; Liang, H.; Chen, K. Effect of Igneous Intrusions on Low-temperature Oxidation Characteristics of Coal in Daxing Mine, China. *Combust. Sci. Technol.* **2021**, *193*, 577–593.
9. Goodarzi, F.; Gentzis, T.; Grasby, S.-E.; Dewing, K. Influence of igneous intrusions on thermal maturity and optical texture: Comparison between a bituminous marl and a coal seam of the same maturity. *Int. J. Coal Geol.* **2018**, *198*, 183–197.

10. Rahman, M.W.; Rimmer, S.M. Effects of rapid thermal alteration on coal: Geochemical and petrographic signatures in the Springfield (No. 5) Coal, Illinois Basin. *Int. J. Coal Geol.* **2014**, *131*, 214–226. [[CrossRef](#)]
11. Qin, Y.; Jin, K.; Tian, F.; Su, W.; Ren, S. Effects of ultrathin igneous sill intrusion on the petrology, pore structure and ad/desorption properties of high volatile bituminous coal: Implications for the coal and gas outburst prevention. *Fuel* **2022**, *316*, 123340. [[CrossRef](#)]
12. He, J.; Wang, B.; Lu, Z. Experimental study on the effect of magma intrusion and temperature on the pore structure of coal. *Energy* **2023**, *284*, 128688. [[CrossRef](#)]
13. Jiang, J.; Zhang, Q.; Cheng, Y.; Jin, K.; Zhao, W.; Guo, H. Influence of thermal metamorphism on CBM reservoir characteristics of low-rank bituminous coal. *J. Nat. Gas Sci. Eng.* **2016**, *36*, 916–930. [[CrossRef](#)]
14. Wang, D.; Song, Y.; Xu, H.; Ma, X.; Zhao, M. Numerical modeling of thermal evolution in the contact aureole of a 0.9 m thick dolerite dike in the Jurassic siltstone section from Isle of Skye, Scotland. *J. Appl. Geophys.* **2013**, *89*, 134–140. [[CrossRef](#)]
15. Yao, Y.; Liu, D. Effects of igneous intrusions on coal petrology, pore-fracture and coalbed methane characteristics in Hongyang, Handan and Huaibei coalfields, North China. *Int. J. Coal Geol.* **2012**, *96–97*, 72–81. [[CrossRef](#)]
16. Wang, L.; Cheng, L.-B.; Cheng, Y.-P.; Yin, G.-Z.; Xu, C.; Jin, K.; Yang, Q.-L. Characteristics and evolutions of gas dynamic disaster under igneous intrusions and its control technologies. *J. Nat. Gas Sci. Eng.* **2014**, *18*, 164–174. [[CrossRef](#)]
17. Li, J.; Zhou, F.; Liu, Y. Effect of magmatic intrusion on coal pore characteristics and fractal research. *J. Min. Sci.* **2015**, *51*, 743–754. [[CrossRef](#)]
18. Li, W.; Zhu, Y.; Chen, S.; Wang, H. Response of coal reservoir porosity to magma intrusion in the Shandong Qiwu Mine, China. *Min. Sci. Technol.* **2011**, *21*, 185–190. [[CrossRef](#)]
19. Cao, D.; Zhan, W.-F.; Li, X.-M. Effect of intrusion of the Shangcheng granite body on structural framework of the Yangshan coal-bearing series, the Beihuaiyang area, China. *J. China Univ. Min. Technol.* **2007**, *36*, 320–324.
20. Shi, Q.; Qin, B.; Liang, H.; Gao, Y.; Bi, Q.; Qu, B. Effects of igneous intrusions on the structure and spontaneous combustion propensity of coal: A case study of bituminous coal in Daxing Mine, China. *Fuel* **2018**, *216*, 181–189. [[CrossRef](#)]
21. Singh, R.-N.; Shonhardt, J.-A.; Terezopoulos, N. A new dimension to studies of spontaneous combustion of coal. *Miner. Resour. Eng.* **2002**, *11*, 147–163. [[CrossRef](#)]
22. Ma, L.; Zou, L.; Ren, L.-F.; Chung, Y.-H.; Zhang, P.-Y.; Shu, C.-M. Prediction indices and limiting parameters of coal spontaneous combustion in the Huainan mining area in China. *Fuel* **2020**, *264*, 116883. [[CrossRef](#)]
23. Zhao, J.; Deng, J.; Chen, L.; Wang, T.; Song, J.; Zhang, Y.; Shu, C.-M.; Zeng, Q. Correlation analysis of the functional groups and exothermic characteristics of bituminous coal molecules during high-temperature oxidation. *Energy* **2019**, *181*, 136–147.
24. Deng, C.-B.; Shan, Y.-F.; Hong, L.; Lu, W.-D. New classifying method of the spontaneous combustion tendency. *J. China Coal Soc.* **2008**, *33*, 47–50.
25. Pan, R.-K.; Li, C.; Yu, M.-G.; Xiao, Z.-J.; Fu, D. Evolution patterns of coal micro-structure in environments with different temperatures and oxygen conditions. *Fuel* **2019**, *261*, 116425. [[CrossRef](#)]
26. Zhang, Y.; Chen, L.; Zhao, J.; Deng, J.; Yang, H. Evaluation of the spontaneous combustion characteristics of coal of different metamorphic degrees based on a temperature-programmed oil bath experimental system. *J. Loss Prev. Process -Dustries* **2019**, *60*, 17–27. [[CrossRef](#)]
27. Zheng, Y.; Li, Q.; Zhang, G.; Zhao, Y.; Zhu, P.; Ma, X.; Liu, X. Effect of multi-component gases competitive adsorption on coal spontaneous combustion characteristics under goaf conditions. *Fuel Process. Technol.* **2020**, *208*, 106510. [[CrossRef](#)]
28. Wang, Y.; Wu, J.; Xue, S.; Wang, J.; Zhang, Y. Experimental Study on the Molecular Hydrogen Release Mechanism during Low-Temperature Oxidation of Coal. *Energy Fuels* **2017**, *31*, 5498–5506. [[CrossRef](#)]
29. Zhong, X.; Kan, L.; Xin, H.; Qin, B.; Dou, G. Thermal effects and active group differentiation of low-rank coal during low-temperature oxidation under vacuum drying after water immersion. *Fuel* **2019**, *236*, 1204–1212. [[CrossRef](#)]
30. Li, K.; Khanna, R.; Zhang, J.; Barati, M.; Liu, Z.; Xu, T.; Yang, T.; Sahajwalla, V. Comprehensive Investigation of Various Structural Features of Bituminous Coals Using Advanced Analytical Techniques. *Energy Fuels* **2015**, *29*, 7178–7189. [[CrossRef](#)]
31. GB/T 474-2008; Method for preparation of coal sample. National Coal Standardization Technical Committee: Beijing, China, 2008.
32. Su, H.; Zhou, F.; Li, J.; Qi, H. Effects of oxygen supply on low-temperature oxidation of coal: A case study of Jurassic coal in Yima, China. *Fuel* **2017**, *202*, 446–454. [[CrossRef](#)]
33. Wang, G.; Yan, G.; Zhang, X.; Du, W.; Huang, Q.; Sun, L.; Zhang, X. Research and development of foamed gel for controlling the spontaneous combustion of coal in coal mine. *J. Loss Prev. Process. Ind.* **2016**, *44*, 474–486. [[CrossRef](#)]
34. Kim, J.; Lee, Y.; Ryu, C.; Park, H.Y.; Lim, H. Low-temperature reactivity of coals for evaluation of spontaneous combustion propensity. *Korean J. Chem. Eng.* **2015**, *32*, 1297–1304. [[CrossRef](#)]
35. Wang, J.; Zhang, Y.; Xue, S.; Wu, J.; Tang, Y.; Chang, L. Assessment of spontaneous combustion status of coal based on relationships between oxygen consumption and gaseous product emissions. *Fuel Process. Technol.* **2018**, *179*, 60–71. [[CrossRef](#)]
36. Li, Z.; Zhang, M.; Yang, Z.; Liu, Y.; Yu, J. Exothermic characteristics of coal during low-temperature oxidation based on grey correlation method. *Energy Rep.* **2022**, *8*, 6744–6752. [[CrossRef](#)]
37. Xu, J.; Ge, L.; He, D. Study on the process of low temperature spontaneous combustion of coal. *Coal Eng.* **1989**, *5*, 7–13.
38. Yang, Y.; Li, Z.; Si, L.; Hou, S.; Li, Z.; Li, J. Study on test method of heat release intensity and thermophysical parameters of loose coal. *Fuel* **2018**, *229*, 34–43. [[CrossRef](#)]
39. Wang, C.-P.; Zhao, X.-Y.; Bai, Z.-J.; Deng, J.; Shu, C.-M.; Zhang, M. Comprehensive index evaluation of the spontaneous combustion capability of different ranks of coal. *Fuel* **2021**, *291*, 120087. [[CrossRef](#)]

40. Zhang, Y.; Zhang, Y.; Li, Y.; Li, Q.; Zhang, J.; Yang, C. Study on the characteristics of coal spontaneous combustion during the development and decaying processes. *Process. Saf. Environ. Prot.* **2020**, *138*, 9–17. [[CrossRef](#)]
41. Yan, H.; Nie, B.; Kong, F.; Liu, Y.; Liu, P.; Wang, Y.; Chen, Z.; Yin, F.; Gong, J.; Lin, S.; et al. Experimental investigation of coal particle size on the kinetic properties of coal oxidation and spontaneous combustion limit parameters. *Energy* **2023**, *270*, 126890. [[CrossRef](#)]
42. Xin, Y.I.; Bai, Z.J.; Xiao, Y.; Wang, C.P.; Deng, J.; Chen, L.G. Impact of imidazole ionic liquid on the maximal limit parameters of the coal spontaneous combustion. *J. Saf. Environ.* **2018**, *18*, 1805–1810. [[CrossRef](#)]
43. Tan, B.; Hu, R.; Li, K.; Bao, T.; Fan, W. Comparison analysis on spontaneous combustion limit parameters of bituminous coal with different metamorphic degree. *Coal Sci. Technol.* **2013**, *41*, 63–67. [[CrossRef](#)]
44. Zhou, F.; Ren, W.; Wang, D.; Song, T.; Li, X.; Zhang, Y. Application of three-phase foam to fight an extraordinarily serious coal mine fire. *Int. J. Coal Geol.* **2006**, *67*, 95–100. [[CrossRef](#)]
45. Li, Q.-W.; Xiao, Y.; Wang, C.-P.; Deng, J.; Shu, C.-M. Thermokinetic characteristics of coal spontaneous combustion based on thermogravimetric analysis. *Fuel* **2019**, *250*, 235–244. [[CrossRef](#)]
46. Xi, Z.; Shan, Z.; Li, M.; Wang, X. Analysis of Coal Spontaneous Combustion by Thermodynamic Methods. *Combust. Sci. Technol.* **2020**, *193*, 2305–2330. [[CrossRef](#)]
47. Qi, X.; Li, Q.; Zhang, H.; Xin, H. Thermodynamic characteristics of coal reaction under low oxygen concentration conditions. *J. Energy Inst.* **2017**, *90*, 544–555. [[CrossRef](#)]
48. Duan, W.; Yu, Q.; Xie, H.; Qin, Q. Pyrolysis of coal by solid heat carrier-experimental study and kinetic modeling. *Energy* **2017**, *135*, 317–326. [[CrossRef](#)]
49. Wang, R.; Liu, G. Variations of concentration and composition of polycyclic aromatic hydrocarbons in coals in response to dike intrusion in the Huainan coalfield in eastern China. *Org. Geochem.* **2015**, *83–84*, 202–214. [[CrossRef](#)]
50. Zhang, X.; Zou, J.; Lu, B.; Huang, G.; Yu, C.; Liang, H. Experimental study on effect of mudstone on spontaneous combustion of coal. *Energy* **2023**, *285*, 128784. [[CrossRef](#)]
51. Xu, C.; Cheng, Y.; Wang, L.; Zhou, H. Experiments on the effects of igneous sills on the physical properties of coal and gas occurrence. *J. Nat. Gas Sci. Eng.* **2014**, *19*, 98–104. [[CrossRef](#)]
52. He, X.; Liu, X.; Nie, B.; Song, D. FTIR and Raman spectroscopy characterization of functional groups in various rank coals. *Fuel* **2017**, *206*, 555–563. [[CrossRef](#)]
53. Wang, S.; Tang, Y.; Schobert, H.H.; Guo, Y.; Su, Y. FTIR and <sup>13</sup>C NMR Investigation of Coal Component of Late Permian Coals from Southern China. *Energy Fuels* **2011**, *25*, 5672–5677. [[CrossRef](#)]
54. Zhao, J.-Y.; Zhang, Y.-L.; Song, J.-J.; Zhang, T.-H.; Ming, H.-Q.; Lu, S.-P.; Deng, J.; Shu, C.-M. Microstructure of coal spontaneous combustion in low-oxygen atmospheres at characteristic temperatures. *Fuel* **2021**, *309*, 122132. [[CrossRef](#)]
55. Shi, Q.; Qin, B.; Bi, Q.; Qu, B. An experimental study on the effect of igneous intrusions on chemical structure and combustion characteristics of coal in Daxing Mine, China. *Fuel* **2018**, *226*, 307–315. [[CrossRef](#)]
56. Ge, L.; Zhang, Y.; Wang, Z.; Zhou, J.; Cen, K. Effects of microwave irradiation treatment on physicochemical characteristics of Chinese low-rank coals. *Energy Convers. Manag.* **2013**, *71*, 84–91. [[CrossRef](#)]
57. Yu, Y.; Liang, W.; Hu, Y.; Meng, Q. Study of micro-pores development in lean coal with temperature. *Int. J. Rock Mech. Min. Sci. Géoméch. Abstr.* **2012**, *51*, 91–96. [[CrossRef](#)]
58. Jiang, J.-Y.; Cheng, Y.-P.; Wang, L.; Li, W.; Wang, L. Petrographic and geochemical effects of sill intrusions on coal and their implications for gas outbursts in the Wolonghu Mine, Huaibei Coalfield, China. *Int. J. Coal Geol.* **2011**, *88*, 55–66. [[CrossRef](#)]
59. Dias, R.-F.; Lewan, M.-D.; Birdwell, J.-E.; Kotarba, M.J. Differentiation of pre-existing trapped methane from thermogenic methane in an igneous-intruded coal by hydrous pyrolysis. *Org. Geochem.* **2014**, *67*, 1–7. [[CrossRef](#)]
60. Karsner, G.-G.; Perlmutter, D.-D. Reaction regimes in coal oxidation. *AIChE J.* **1981**, *27*, 920–927. [[CrossRef](#)]
61. Kaji, R.; Hishinuma, Y.; Nakamura, Y. Low temperature oxidation of coals: Effects of pore structure and coal composition. *Fuel* **1985**, *64*, 297–302. [[CrossRef](#)]
62. Tang, Y.; Xue, S. Laboratory Study on the Spontaneous Combustion Propensity of Lignite Undergone Heating Treatment at Low Temperature in Inert and Low-Oxygen Environments. *Energy Fuels* **2015**, *29*, 4683–4689. [[CrossRef](#)]
63. Saghafi, A.; Faiz, M.; Roberts, D. CO<sub>2</sub> storage and gas diffusivity properties of coals from Sydney Basin, Australia. *Int. J. Coal Geol.* **2007**, *70*, 240–254. [[CrossRef](#)]
64. Jiang, J.; Cheng, Y. Effects of Igneous Intrusion on Microporosity and Gas Adsorption Capacity of Coals in the Haizi Mine, China. *Sci. World J.* **2014**, *2014*, 976512–976582. [[CrossRef](#)] [[PubMed](#)]
65. Lu, W.; Cao, Y.-J.; Tien, J.C. Method for prevention and control of spontaneous combustion of coal seam and its application in mining field. *Int. J. Min. Sci. Technol.* **2017**, *27*, 839–846. [[CrossRef](#)]

**Disclaimer/Publisher’s Note:** The statements, opinions and data contained in all publications are solely those of the individual author(s) and contributor(s) and not of MDPI and/or the editor(s). MDPI and/or the editor(s) disclaim responsibility for any injury to people or property resulting from any ideas, methods, instructions or products referred to in the content.